Performance of the Helical Coils for the Large Helical Device in Six Years' Operation

S. Imagawa, N. Yanagi, H. Sekiguchi, T. Mito, and O. Motojima

***Abstract*—A pair of helical coils of the Large Helical Device is the largest pool-cooled superconducting magnet. The first excitation test up to 1.5 T was carried out at the end of March, 1998. In the first trial to charge up to the design value of 3 T, wide propagation of a normal-zone was induced at 11.45 kA, and the quench detection system acted. It was revealed that a normal-zone could propagate below the cold-end recovery current by additional heat generation due to the slow current diffusion into the thick pure aluminum stabilizer. In these six years' operation, propagation of a normal-zone has been observed 17 times at almost the same current. The normal-zones were recovered within several seconds except for the wide propagation. By a novel detection system of the propagation with pick-up coils along the helical coils, it was disclosed that the recovered normal-zones propagated in only one side. In order to attain plasma experiments near 3 T, higher excitations were tried by the current grading method, in which the current of the innermost block is decreased and those of the other two blocks are increased. The average current of 11.67 kA was attained. The excitation tests up to the highest currents have been carried out after each cool-down. Degradation is not observed in the coil performance, and the stable operation has been demonstrated.**

***Index Terms*—Aluminum stabilizer, balance voltage, conductor motion, helical coil.**

I. Introduction

THE LARGE Helical Device (LHD) is the largest stellarator, which is utilized for the research of fusion plasma near a reactor region [1]. Superconducting magnets are adopted in order to demonstrate steady-state operation. The magnet system consists of a pair of pool-cooled helical coils and three pairs of poloidal coils made of cable-in-conduit conductors, as shown in Fig. 1 [2]. The major and minor radii of the helical coil are 3.9 and 0.975 m, respectively.

The first cool-down was successfully carried out from the middle of February in 1998. The coils were excited up to 1.5 T, which is half of the design field, and preliminary plasma experiments were carried out to check the soundness of the whole system. After that, the coils were warmed up for upgrading the plasma-heating devices. The second cool-down was performed from the middle of August. Excitation up to the design value of 3 T was tried in October. A wide propagation of a normal-zone was observed in the helical coil at 11.45 kA, and the quench detection system acted [3]. The protection circuit worked correctly. Although the helical coil was designed to be cryostable, it was revealed that a normal-zone could propagate below the cold-end recovery current. The main reason is additional heat generation due to the slow current diffusion into the thick pure aluminum stabilizer [4]. Since the quality of liquid helium may affect the cryostability, the charging rate was lowered from 0.1 T/min to 0.01 or 0.02 T/min at currents higher than 10.8 kA. In spite of that, the propagation and recovery have been observed repeatedly at almost the same currents [5]. From the measurement with pickup coils along the helical coils, it was revealed that the recovered normal-zones propagated to only one side. The asymmetry of the propagation of a normal-zone is caused by electromagnetic interaction [6]. A higher excitation was tried by the current grading method, in which the current of the innermost block is decreased and those of the other two blocks are increased. The average current of 11.67 kA was attained, and plasma experiments at 2.89 T of the central toroidal field have been carried out. Seven cool-down and over 700 excitation cycles have been achieved in six years' operation. No degradation is observed in the coil performance, and stable operations have been demonstrated. This paper will summarize the status of the helical coils and the understanding about the cryostability and the conductor motions.

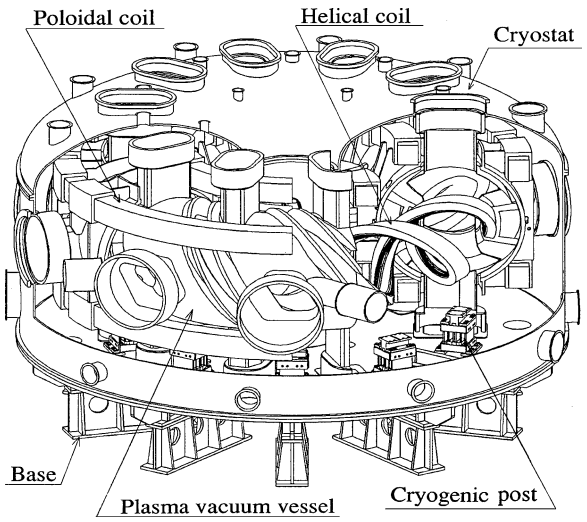

Fig. 1. Whole assembly of a cryostat and a plasma vacuum vessel of LHD.

II. Helical Coil System of LHD

A. Design of Helical Coil

The helical coil rotates five times around a plasma vacuum vessel, as shown in Fig. 1. Conductors are packed in the coil cases which are fixed from a cylindrical supporting shell, as shown in Fig. 2. The conductor consists of NbTi/Cu strands, a

Manuscript received October 20, 2003.

The authors are with the National Institute for Fusion Science, 322-6 Oroshi-cho, Toki, Gifu 509-5292, Japan (e-mail: imagawa@LHD.nifs.ac.jp).

Digital Object Identifier 10.1109/TASC.2004.830583

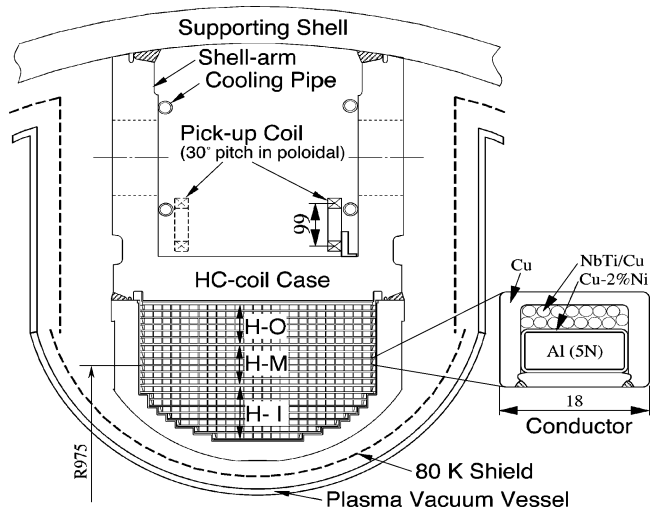

Fig. 2. Cross-sectional view of the LHD and the helical coils. The pick-up coils are arranged by the pitch of 30 degree of the poloidal angle at the right or left side alternately inside the shell-arms.

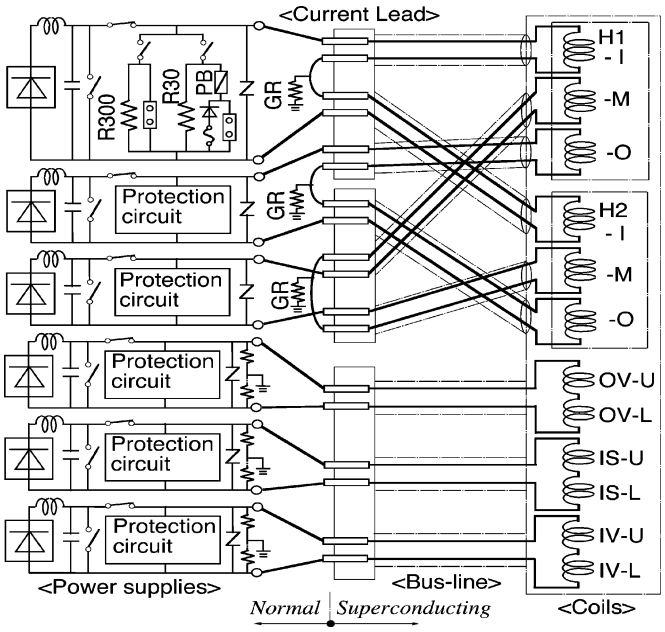

Fig. 3. Circuit diagram of the power line of the helical coils for LHD.

pure aluminum stabilizer, and a copper sheath for the high cryogenic stability and the necessary mechanical strength. Glass-fiber-reinforced-plastics spacers are inserted between the conductors by certain intervals for electrical insulation. The wetted surface fraction varies from 0.4 to 0.67, as the highest pressure on the spacers by the electromagnetic force does not exceed 100 MPa at the central toroidal field of 4 T [7].

The helical coil is divided into three blocks to reduce the shut-off voltage and to change the minor radius of the current center of the coil. The blocks are called I, M, and O from the inside. The same named blocks in H1 and H2 coils are usually connected in series, as shown in Fig. 3. Each power supply has its own local control unit, and the necessary voltage is calculated every 20 ms by the central control unit to minimize the current errors [8]. A simple P control scheme is adopted in the normal operation, and the feedback gain K_p is set to 0.1 to prevent oscillating. A current error less than 0.2% is achieved for the helical coils, and the time constant of feedback control of the current is about 10 s.

Liquid helium is supplied from ten positions at the bottom of the two helical coils, and the generated gas is taken out from the ten top positions to a header tank. Longitudinal cooling channels inside the coils are arranged at the higher side of each layer and both corners of the top cover of the case. The cross-sectional areas of the channels are 34 mm^2 per layer and 300 mm^2 per corner, respectively. The area was designed for steady heat input and AC losses in charging, which are in the range of 100 W. Thus, the cooling condition can be deteriorated by accumulation of helium bubbles in the case of the propagation of a normal-zone.

B. Pick-Up Coils and Other Sensors

Sensors are not installed in the coils to avoid troubles due to the cables or feed-throughs. Voltage taps are attached on the copper bar jointing the coil leads and the superconducting bus-lines. The coil cases are equipped with 38 temperature sensors, 45 strain gauges and 10 Hall probes. Temperature sensors are attached on the joint pieces. Acoustic emission sensors have been installed before the seventh cooling cycle.

In order to detect the induced position of a normal-zone, pick-up coils have been installed along the helical coil, as shown in Fig. 2, after the fourth cycle. Those are arranged by the pitch of 30 degree of the poloidal angle at the right or left side alternately inside the shell-arms. The pick-up coils are designed to detect the change of magnetic field by current transfer between the superconducting strands and the aluminum stabilizer at the front and end of a normal-zone. The turn number of the pick-up coil is 10 000. The output of each pick-up coil on the H1 coil is balanced by that on the H2 coil at the opposite toroidal angle. The signals are acquired with a sampling rate of 50 Hz with the low-pass filter of 30 Hz.

C. Balance Voltage

The balance voltage is the voltage of H1 coil minus H2 coil for each block. Since the three blocks are strongly coupled, the state of conductor motions or a normal-zone propagating is analyzed by evaluation of the difference among the three balance voltages. In the case of conductor motions by electromagnetic force under the constant current, positive voltage is induced in all the three blocks because the coil inductance is enlarged. The voltage becomes the highest in the block that contains the moved conductor [9].

When a normal-zone propagates, the current diffuses into the aluminum stabilizer from the superconducting strands. An inductance change is induced by the geometrical shift of the current. In this case, no mechanical work is induced. Hence, this is equivalent to add a new circuit [9]. When a normal-zone propagates in the I-block, the voltage drop due to the resistance of the normal-zone e_R is expressed as,

$$e_R = e_I - \frac{B_I I_M}{B_M I_I} e_M \equiv e_I - \frac{e_M}{\alpha}, \tag{1}$$

where e_j and I_j are the balance voltage and the current of j ($j =$ I, M, O) block, respectively. B_j is the magnetic field den-

TABLE I
MAX. AND MIN. RATIO OF THE MAGNETIC FIELD IN THE OVERTURNING DIRECTION BY M-BLOCK TO THAT OF BY I-BLOCK

Turn	L8	L7	L6	L5	L4	L3	L2	L1
T1	-3.47							Max.
	-9.32							Min.
T2	-2.22	139	3.49					
	-3.64	-221	2.61					
T3	-1.87	-4.95	6.4	1.78				
	-2.74	-16.7	3.76	1.62				
T4	-1.67	-3.54	19.1	2.36	**1.24**			
	-2.36	-7.40	5.84	2.00	**1.19**			
T5	-1.56	-2.94	746	3.07	1.45	**0.94**		
	-2.14	-5.20	-121	2.40	1.35	**0.93**		
T6	-1.48	-2.57	2380	3.85	1.60	0.96		
	-1.98	-4.23	-92.8	2.86	1.47	0.95		
T7	-1.42	-2.36	530	4.93	1.81	1.09	0.79	
	-1.88	-3.64	-2691	3.33	1.63	1.06	0.78	
T8	-1.37	-2.20	-6.21	6.40	2.02	1.17	0.81	
	-1.80	-3.31	-32	3.86	1.77	1.13	0.80	
T9	-1.34	-2.10	-5.35	8.09	2.22	**1.25**	**0.87**	0.69
	-1.74	-3.09	-17.6	4.43	1.90	**1.19**	**0.86**	0.67
T10	-1.31	-2.03	-4.81	10.16	2.37	**1.31**	**0.89**	0.68
	-1.70	-2.95	-13.2	4.91	2.01	**1.24**	**0.89**	0.67
T11	-1.30	-1.98	-4.54	12.14	2.47	1.34	**0.90**	0.68
	-1.67	-2.85	-11.2	5.27	2.07	1.26	**0.89**	0.67
T12	-1.29	-1.96	-4.39	13.41	2.52	1.35	**0.90**	0.68
	-1.65	-2.80	-10.5	5.51	2.11	1.27	**0.90**	0.67
T13	-1.28	-1.95	-4.35	13.94	2.54	1.36	**0.91**	0.68
	-1.65	-2.78	-10.2	5.58	2.12	1.28	**0.90**	0.67

sity by j-block across the additional circuit by the current shift. The ratios of magnetic field at each turn by M-block to that by I-block are shown in Table I.

Since the balance voltage of M-block is only the inductive component, the propagation velocity is estimated from it. Then, e_R is estimated by the other equation,

$$e_R = -\frac{r \cdot I_M}{\alpha \cdot B_M} \int e_M dt = -\beta \int e_M dt, \qquad (2)$$

where r and a are the resistance of the conductor per unit length and the distance of the current shift, respectively. In the helical coil, a is 4.5 mm, and r is around 0.7 $\mu\Omega/\mathrm{m}$.

The factor α and β are evaluated by matching the waveforms derived from (1) and (2). The cross-sectional position of the normal-zone can be estimated from the factor α.

III. EXCITATION PROPERTIES OF HELICAL COIL

A. Conductor Motions

An example of the balance voltage in charging and discharging is shown in Fig. 4. The spike voltages appear frequently from about 8 kA in a charging process and these disappear while holding the current or discharging to about 9 kA [10]. These spike voltages could be induced by conductor motions that have hysteresis. The major voltages may be induced by the conductors sliding onto the coil case. Since the conductor moves to increase the coil inductance, positive or negative voltage corresponds to the motion in H1 or H2 coil, respectively. Besides, the balance voltages with fixed shapes appear when changing the ramp rate of the current. These are considered to be induced by the secondary circuits such as the helical coil cases and the supporting structures.

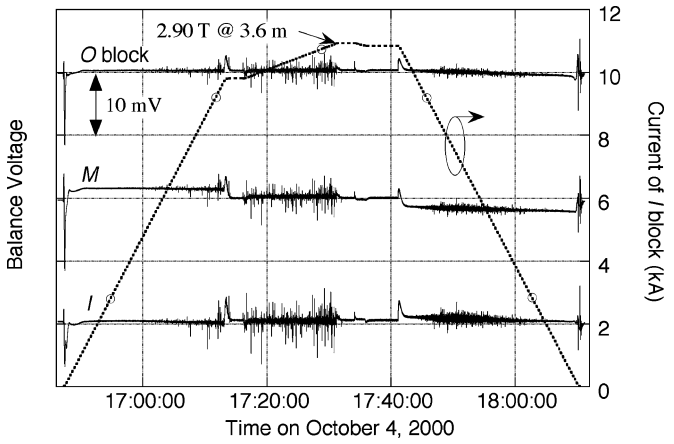

Fig. 4. Balance voltages of the helical coils during a charge and a discharge up to average 11.60 kA on October 4, 2000.

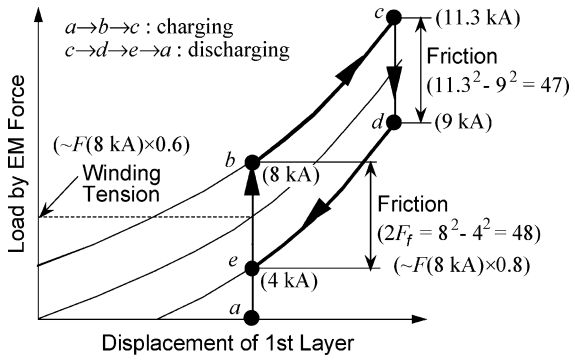

Fig. 5. Schematic drawing of the relation between the displacement of conductor and the electromagnetic force during charging and discharging.

The mechanism of the hysteresis can be explained by taking account of winding tension besides friction to the coil case, as shown in Fig. 5. In charging process, the conductors begin sliding outwards on the coil case when the electromagnetic force exceeds the winding tension plus the friction. In discharging process, the conductors do not slide until the decrease of electromagnetic force exceeds the twice of the friction.

The spike voltages are coincidentally observed in the three blocks, and the major voltages of I-block are always higher than the other blocks. Therefore, apparent conductor motions are induced in only the I-block. From the comparison of charging and discharging processes, the spike voltages in discharging are obviously lower and more frequent than those in charging. Consequently, the conductors move back smoothly in a discharging process.

B. Propagation of a Normal-Zone

Major excitation tests and the propagation of normal-zones are listed in Table II. The propagation of a normal-zone has been observed 17 times until the half of seventh cooling cycle. 12 times were in the H1 coil. All the normal-zones were induced in the I-block including the current grading excitations, in which the current of the I-block is lower than the others. The factor α and β are shown in Table III. All the normal components estimated by (1) are shown in Fig. 6.

Since the factors in all the propagation in the H1-I block are same, normal-zones should be induced in the same layer and

TABLE II
MAJOR EXCITATION TESTS UP TO THE HALF OF THE SEVENTH COOLING CYCLES

Date	Current (central field @ major radius)
Mar. 27 '98	6.50 kA (1.56 T @ 3.75 m)
Oct. 20 '98	10.41 kA (2.50 T @ 3.75 m)
Oct. 21	11.25 kA (2.70 T @ 3.75 m) #1 propagation in H1
	11.3 kA (2.71 T @ 3.75 m) #2 propagation in H2
	11.4 kA (2.74 T @ 3.75 m) #3 propagation in H2
	11.45 kA (2.75 T @ 3.75 m) #4 propagation in H1
Dec. 17	11.41 kA (2.74 T @ 3.75 m), 11.40 kA (2.85 T @ 3.60 m)
Dec. 18	11.45 kA (2.75 T @ 3.75 m)
July 21 '99	11.33 kA (2.72 T @ 3.75 m) #5 propagation in H1
Aug. 6	11.40 kA (2.85 T @ 3.60 m)
Sep. 9	11.27 kA (2.90 T @ 3.50 m)
Nov. 30	av. 11.65 kA (2.91 T @ 3.60 m) #6 propagation in H1
	[I/M/O = 11.08 / 11.84 / 12.03 kA]
Dec. 15	11.41 kA (2.74 T @ 3.75 m)
	av. 11.65 kA (2.91 T @ 3.60 m) #7 propagation in H1
Sep. 27 '00	11.33 kA (2.72 T @ 3.75 m)
Sep. 28	av. 11.64 kA (2.91 T @ 3.6 m) #8 propagation in H1
	[I/M/O = 10.975 / 11.873 / 12.072 kA]
Oct. 4	av. 11.62 kA (2.906 T @ 3.6 m) #9 propagation in H2
Dec. 1	av. 11.64 kA (2.91 T @ 3.6 m) 3 times
Sep. 18 '01	11.33 kA (2.72 T @3.75 m), av. 11.64 kA (2.99 T @3.5 m)
Nov. 29	av. 11.67 kA (2.917 T @3.6 m) [I/M/O=11.0 / 11.9 / 12.1 kA]
Dec. 18	-11.30 kA (-2.825 T @3.6 m), av. -11.64 kA (-2.91 T @3.6 m)
Sep. 27 '02	11.16 kA (2.45 T @ 4.1 m) #10 propagation in H1
Nov. 6	av. 11. 5 kA (2.76 T @ 3.75 m) #11 propagation in H1
Nov. 28	11.04 kA (2.65 T @ 3.75 m) #12 propagation in H1
Dec. 6	11.15 kA (2.68 T @ 3.75 m) #13 propagation in H1
Dec. 12	11.30 kA (2.825 T @ 3.6 m) #14 propagation in H1
Dec. 25	-11.08 kA (-2.558 T @ 3.9 m) #15 propagation in H2
Feb. 5	-11.11 kA (-2.67 T @ 3.75 m) #16 propagation in H2
Sep. 5	11.00 kA (-2.44 T @ 4.05 m) #17 propagation in H1

(*1) A normal-zone recovered except for the #4 propagation.

TABLE III
SUITABLE FACTOR FOR THE PROPAGATION OF A NORMAL-ZONE

No.	Mode	Current (kA)	Coil	position	α	β
1	#1-o_2.70 T	11.25	H1-I	-	0.9	1.1
2	#1-o_2.71 T	11.29	H2-I	-	0.9	0.9
3	#1-o_2.74 T	11.41	H2-I	-	1.2	1.4
4	#1-o_2.75 T	11.45	H1-I	-	0.9	1.1
5	#1-o_2.72 T	11.33	H1-I	-	0.9	1.1
6	#1-d_2.91 T_γ1.258	11.07	H1-I	-	0.9	1.1
7	#1-d_2.91 T_γ1.258	11.07	H1-I	-	0.9	1.1
8	#1-d_2.91 T_γ1.258	10.97	H1-I	-	0.9	1.1
9	#1-d_2.906 T_γ1.258	10.95	H2-I	-	1.25	1.4
10	#1-c_R4.1 m_2.45 T	11.16	H1-I	#10 bottom	0.9	0.9
11	#1-o_2.74 T_γ1.258	10.94	H1-I	#10 bottom	0.9	0.9
12	#1-o_2.65 T	11.04	H1-I	#10 bottom	0.9	0.9
13	#1-o_2.68 T	11.15	H1-I	#10 bottom	0.9	0.9
14	#1-d_2.825 T	11.30	H1-I	#10 bottom	0.9	0.9
15	#1-c_-2.558 T	-11.08	H2-I	#5 bottom	0.9	1.0
16	#1-o_-2.67 T	-11.11	H2-I	#5 bottom	0.9	1.0
17	#1-c_R4.05 m_2.44 T	11.00	H1-I	#10 bottom	0.9	0.9

turn. The factor of α of 0.9 means that the normal-zones may have been induced at the side end of the third layer or the middle of the second layer from the Table I. Considering the possibility of large conductor motions, the side end of the third layer is the probable position, because the conductors at the end of the layers can slide against the coil case. The third and ninth propagation may have occurred at the end of the fourth layer of the H2 coil. The high value of β may be caused by the high resistance of the conductor. The 2nd, 15th and 16th propagation may have occurred at the side end of the third layer of the H2 coil.

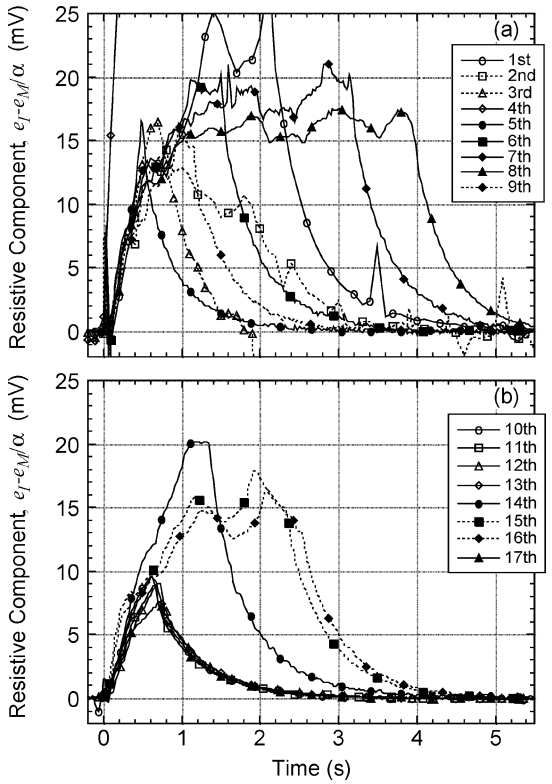

Fig. 6. The estimated normal components for 17 times propagation of a normal-zone.

In the sixth campaign, the propagation of normal-zones has been induced seven times that are the 10th to 16th propagation from the first cycle. The position and the velocity of the propagation were detected successfully with the pick-up coils. The 10th normal-zone was initiated at the bottom of #10 section. The following four normal-zones were initiated at the same or near position. The 15th and 16th normal-zones were induced in the reverse excitation at the bottom of #5 section. All the seven normal-zones propagated in one side, which is the downstream of the transport current, with recovery at the opposite side. The asymmetry of the propagation velocity is considered to be caused by electromagnetic interaction between the transfer current and the magnetic field.

The outputs of the right pick-up coils for the 14th and 15th normal-zone are shown in Fig. 7. The schematic drawing of the position of the normal-zones are shown in Fig. 8. The amplitude of outputs of the left pick-up coils is almost half of that of the right coils. Therefore, the normal-zone were initiated at the right side inside the helical coils, where the magnetic field becomes higher at the inside and bottom position, as shown in Fig. 9. The ripple of the field in a pitch is about 0.4 T. Fig. 7 shows that the propagation of the 14th normal-zone stopped at the top of the next pitch, which is the lower field area. The 10th to 13th normal-zones also stopped at the top position within a pitch; that is, the propagation length is almost the half pitch. On the other hands, the 15th and 16th normal-zones propagated almost three pitches, and these stopped near the layer to layer joint, which is located outside of the torus. The propagation velocity was 7 to 9 m/s, which become faster at higher currents. In the reverse excitation, the normal-zones propagated beyond

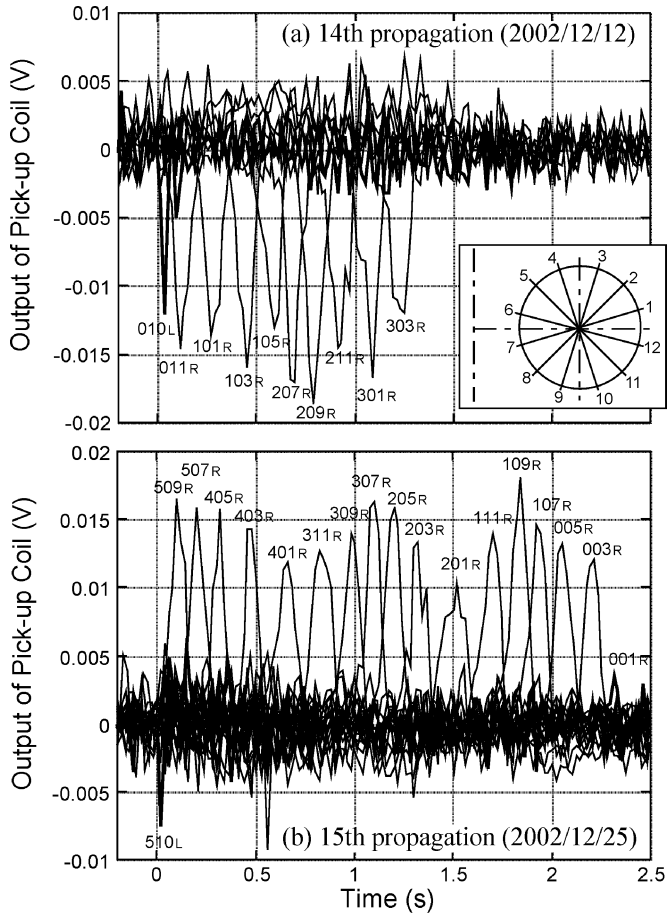

Fig. 7. Outputs of pick-up coils during the 14th (a) and 15th (b) propagation of a normal-zone. Numbers of three figures mean the sector and the poloidal position of the coils.

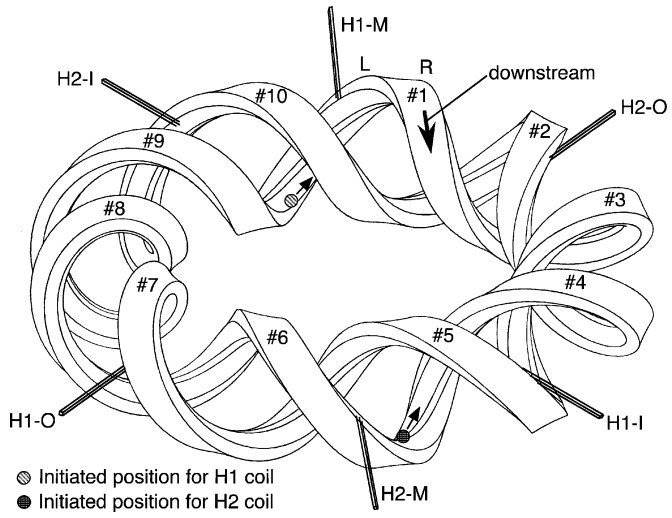

Fig. 8. Initiated positions of normal-zones and the direction of propagation in the sixth cycle.

one pitch in spite of relatively lower currents. The reason is not clear. The cryogenic stability of the H2 coil might be less than H1 coil, or the direction of propagation to the distribution of magnetic field might affect the dynamic heat balance.

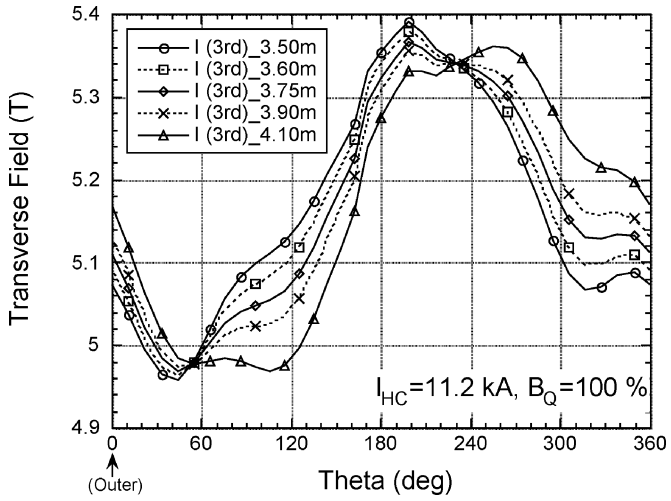

Fig. 9. Transverse magnetic field at the right end of the third layer of the helical coil for plasma axis of 3.42 to 4.10 m.

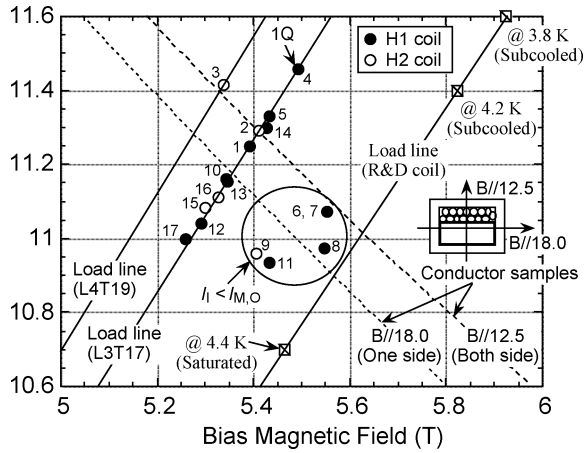

Fig. 10. Maximum transverse magnetic fields at the third and fourth layers for the propagation of normal-zones in LHD.

IV. Discussion

The spike voltages are coincidentally observed in the three blocks. The voltage of the I-block is always higher than the other blocks. Therefore, apparent conductor motion by the electromagnetic force is induced in only the I-block. Since the coil is supported from the top cover, the displacement of the conductor becomes larger in lower layers. The M- and O-blocks should be within an elastic deformation, or the conductor motions might be smoothed by being pressed by the I-block. Assuming that the winding tension and the friction are 60% and 80% of the electromagnetic force at 8 kA as shown in Fig. 5, the fourth layer might start moving at about 11.5 kA.

The normal-zones were speculated to be induced at the side ends of the third and fourth layers from the evaluation of the balance voltages. The currents at the 17 times propagation in the helical coils are plotted in Fig. 10 versus the magnetic field at the third or fourth layer. As compared with the minimum currents for propagation in the conductor tests and in a mock-up coil test, the results of the helical coils seem reasonable. A normal-zone has not been induced in the first or second layer in spite of the higher field. A possible reason is the degradation of properties

of the conductor at the third and fourth layers. However, the characteristic of conductor motions should be the main reason, because the normal-zones are considered to have been induced at the similar positions in both the two helical coils. A large conductor motion is needed to induce the propagation near the threshold current. Such a large disturbance could occur when the conductor slides on the end-spacer for the first time. This is consistent with the above speculation that the third or fourth layer may start moving at about 11 kA.

Since the magnetic field in the M or O-block is lower than the I-block, these blocks should be cryostable at a higher current. Therefore, current grading excitations have been tested. The current of I-block is decreased and the currents of M and O are increased not to exceed the predicted threshold current which is the lowest current for a normal-zone propagating. The average 11.67 kA was achieved with the currents of I-, M-, O-block of 11.0, 11.9, 12.1 kA, respectively. The higher excitation will be achievable by the higher grading ratio. However, it can not be used for plasma experiments because the average coil minor radius becomes too large. In order to improve the cryostability, it is planned to insert an evacuated pre-cooler before the inlet of the coil and to lower the inlet temperature down to 3 K [11]. The stability tests in subcooled helium have been carried out with a mock-up coil [12].

V. Summary

Although the helical coils of the Large Helical Device was designed to satisfy the criteria of the cold-end stability at the design current of 13 kA at 4.4 K, a normal-zone can propagate below the cold-end recovery current by additional heat generation due to the slow current diffusion into the thick pure aluminum stabilizer. The average current of 11.67 kA was attained by the current grading method, in which the current of the innermost block is decreased and those of the other two blocks are increased. In the six years' operation, the propagation of a normal-zone was observed 17 times at about 11 kA. Except for a rapid growth of the normal-zone at 11.45 kA, the other normal-zones were recovered to the superconducting state within several seconds. A novel method with pick-up coils has revealed that the recovered normal-zones propagated in only one side. Besides, the features of conductor motions in charging and discharging have been investigated. Its mechanism can be explained by the friction and the initial winding tension. According to the excitation tests after each cool-down, the performance degradation is not observed in the coil. The stable operation of the large-scale superconducting magnet system has been demonstrated.

Acknowledgment

The authors are indebted to the staff of the LHD project as well as many collaborators from universities.

References

[1] A. Iiyoshi and A. Komori *et al.*, "Overview of the large helical device project," *Nuclear Fusion*, vol. 39, pp. 1245–1256, 1999.

[2] A. Iiyoshi, S. Imagawa, and LHD group, "Design, construction and the first plasma experiments in the large helical device," *Fusion Eng. Des.*, vol. 46, pp. 323–335, Nov. 1999.

[3] S. Imagawa, N. Yanagi, and H. Chikaraishi *et al.*, "Results of the first excitation of helical coils of the large helical device," *IEEE Trans. Appl. Supercond.*, vol. 10, no. 1, pp. 606–609, March 2000.

[4] N. Yanagi, A. V. Gavrilin, and T. Mito *et al.*, "Stability characteristics of the aluminum stabilized superconductor for the LHD helical coils," *Advances in Superconductivity XI*, pp. 991–994, 1999.

[5] S. Imagawa, N. Yanagi, and T. Mito *et al.*, "Excitation properties and cryogenic stability of helical coils for the LHD," *IEEE Trans. Appl. Supercond.*, vol. 11, no. 1, pp. 1889–1892, March 2001.

[6] N. Yanagi, S. Imagawa, and Y. Hishinuma *et al.*, Asymmetrical Normal-Zone Propagation Observed in the Aluminum-Stabilized Superconductor for the LHD Helical Coils, this conference.

[7] S. Imagawa, S. Masuzaki, N. Yanagi, S. Yamaguchi, T. Satow, J. Yamamoto, O. Motojima, and LHD group, "Design and construction of helical coils for LHD," *Fusion Eng. Des.*, vol. 41, pp. 253–258, 1998.

[8] H. Chikaraishi, S. Yamada, O. Motojima, T. Sato, K. Tomatsu, H. Niwa, and T. Haga, "Current control of superconducting coils of LHD," in *Proc. Fusion Technology 1998*, 1998, pp. 759–762.

[9] S. Imagawa, N. Yanagi, H. Sekiguchi, and T. Mito *et al.*, "Consideration for the conductor motions in the helical coils of the large helical device," *IEEE Trans. Appl. Supercond.*, vol. 13, no. 2, pp. 1484–1487, June 2003.

[10] N. Yanagi, S. Imagawa, and S. Hamaguchi *et al.*, "Pulse height analysis of the spike signals on the balance voltage observed in the LHD helical coils," in *Proc. ICEC 18*, Mumbai, 2000, pp. 179–182.

[11] T. Mito, A. Nishinura, and S. Yamada *et al.*, "Design, development and operation of superconducting system for LHD," in *19th IEEE Symposium on Fusion Engineering*, Atlantic City, January 22–25, 2002.

[12] S. Imagawa, N. Yanagi, and Y. Hishinuma *et al.*, Results of Stability Test in Subcooled Helium for the R&D Coil of the LHD Helical Coil, this conference.